BIOCHEMISTRY
including biophysical chemistry & molecular biology

Article

pubs.acs.org/biochemistry

Positional Effects of Phosphorylation on the Stability and Morphology of Tau-Related Amyloid Fibrils

Masafumi Inoue,[†] Takashi Konno,[§] Kazuki Tainaka,[†] Eiji Nakata,[†] Hiro-o Yoshida,[†] and Takashi Morii[†,*,‡]

[†]Institute of Advanced Energy, Kyoto University, Uji, Kyoto 611-0011, Japan

[‡]CREST, JST, Uji, Kyoto 611-0011, Japan

[§]Department of Molecular Physiology and Biophysics, Faculty of Medical Sciences, University of Fukui, Matsuoka, Yoshida, Fukui 910-1193, Japan

Supporting Information

ABSTRACT: Hyperphosphorylated forms of tau protein are the main component of paired helical filaments (PHFs) of neurofibrillary tangles in the brain of Alzheimer's disease patients. To understand the effect of phosphorylation on the fibrillation of tau, we utilized tau-derived phosphorylated peptides. The V_{306}QIVYK$_{311}$ sequence (PHF6) in the microtubule-binding domain is known to play a key role in the fibrillation of tau, and the short peptide corresponding to the PHF6 sequence forms amyloid-type fibrils similar to those generated by full-length tau. We focused on the amino acid residue located at the N-terminus of the PHF6 sequence, serine or lysine in the native isoform of tau, and synthesized the PHF6 derivative peptides with serine or lysine at the N-terminus of PHF6. Peptides phosphorylated at serine and/or tyrosine were synthesized to mimic the possible phosphorylation at these positions. The critical concentrations of the fibrillation of peptides were determined to quantitatively assess fibril stability. The peptide with the net charge of near zero tended to form stable fibrils. Interestingly, the peptide phosphorylated at the N-terminal serine residue exhibited remarkably low fibrillation propensity as compared to the peptide possessing the same net charge. Transmission electron microscopy measurements of the fibrils visualized the paired helical or straight fibers and segregated masses of the fibers or heterogeneous rodlike fibers depending on the phosphorylation status. Further analyses of the fibrils by the X-ray fiber diffraction method and Fourier transform infrared spectroscopic measurements indicated that all the peptides shared a common cross-β structure. In addition, the phosphoserine-containing peptides showed the characteristics of β-sandwiches that could interact with both faces of the β-sheet. On the basis of these observations, possible protofilament models with four β-sheets were constructed to consider the positional effects of the serine and/or tyrosine phosphorylations. The electrostatic intersheet interaction between phosphate groups and the amino group of lysine enhanced the lateral association between β-sheets to compensate for the excess charge. In addition to the previously postulated net charge of the peptide, the position of the charged residue plays a critical role in the amyloid fibrillation of tau.

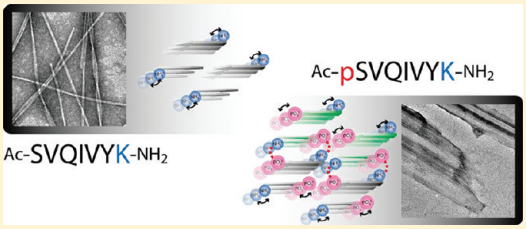

Amyloid-type fibrillation of proteins in the brain is a crucial event for human degenerative diseases.[1,2] Neurofibrillary tangles that comprise paired helical filaments (PHFs) and straight filaments composed mainly of hyperphosphorylated tau protein represent pathological hallmarks of Alzheimer's disease (AD).[3−6] Various inclusions comprised of highly phosphorylated tau play a part in the neuronal loss evident in tauopathies.[7] Thus, phosphorylation and dephosphorylation of human tau protein are believed to be involved in the onset of AD.[8] Phosphorylation of tau at different sites would show diverse effects on the physiological and pathological activities,[9−11] but it is not known whether the differences in the phosphorylation status in tauopathies such as AD or progressive supranuclear palsy (PSP) could affect the formation of different filamentous tau aggregates.[12] For example, PHF and straight filaments are detected in the AD brain,[13] whereas straight filaments are observed in PSP.[14,15] Hyperphosphorylation of tau was reported to enhance fibrillation;[16] however, the detailed mechanisms of how the individual phosphorylation event induces the formation of PHF remain to be established.[17] It has been reported that the salt bridge is important for the stability of fibrils;[18−21] thus, phosphorylation events would directly affect the fibrous assembly of tau. An increasing number of potential phosphorylation sites of tau in the AD brain have been identified, and as many as 45 sites of tau are suggested to be phosphorylated in PHF-tau.[4,22−24] In addition, there may be sites that have not yet been identified.[25]

Tau binds to microtubules through the microtubule-binding domain that contains three or four repeats of 31 or 32 residues, depending on the three-repeat tau splice isoform or the four-repeat tau splice isoform, respectively. The microtubule-binding

Received: September 17, 2011
Revised: January 24, 2012
Published: January 24, 2012

   dx.doi.org/10.1021/bi201451z | *Biochemistry* 2012, 51, 1396−1406

domain of tau is also proposed to be a core nucleation site for formation of amyloid fibrils.[26,27] In the aggregating protein, the core region was reported to consist of four to seven residues that have a high potential to aggregate to fibrils by themselves.[28−33] The usage of short peptide segments of the aggregating core region allows us to investigate the molecular details of amyloid formation. For example, microcrystals of the short amyloidgenic peptides have been utilized to determine atomic structures of many amyloid species,[34] which suggested a rational classification of the amyloid fibril structures.[35] The hexapeptide motif of V_{306}QIVYK$_{311}$ (PHF6) in the microtubule-binding domain of tau protein forms the fibrils with PHF-like morphology.[36,37] It has also been reported that a short peptide PHF6 in the core nucleation site has the greatest amyloid forming potential and the PHF6 peptide and its mutants at the Tyr310 position form amyloid fibrils displaying PHF morphology.[36,38] We have previously investigated the stability and morphology of amyloid fibrils by utilizing the short peptide PHF6 derivatives. When a non-natural derivative of tyrosine, such as 4-phenylphenylalanine or 4-methylphenylalanine, is substituted for Tyr310, the aromatic and hydrophobic non-natural amino acids contributed to the significant enhancement of the amyloid forming propensity.[39]

Phosphorylation of tau within the microtubule-binding domain would reveal functional consequences not only for its microtubule binding but also for its fibril formation activities. The role of specific individual phosphorylation sites for tau function and/or fibril formation remains to be established. We have previously reported that a phosphorylation of Tyr310 within the PHF6 peptide dramatically affects the stability of fibrils by changing its dependency on pH and ionic strength.[20] Under acidic conditions, a phosphotyrosine-containing PHF6 derivative, PHF6pY, shows enhanced fibrillation propensity. The effect of the phosphorylation of Tyr on fibril formation is explained well by the charge compensation upon electrostatic pairing of the phosphate group with the amino group of the neighboring Lys residue.

In this study, we have focused on the positional effect of the phosphate group on the amyloid fibrillation by the PHF6 derivatives of peptides. Ser305 at the N-terminus of the V_{306}QIVYK$_{311}$ sequence is a target of phosphorylation by several kinases, such as casein kinase 1 (CK1), glycogen synthase kinase-3 (GSK-3), and microtubule affinity regulating kinase, known to be activated in AD brain.[25,40,41] Furthermore, Ser305 is substituted with the positively charged Lys residue in the three-repeat tau splice isoform.[42] These variations in electrostatic properties have the potential to change the aggregation property of PHF6. We have synthesized the PHF6 derivative of peptides containing seven residues with an additional Ser, phosphoserine, or Lys at the N-terminus of PHF6, and their Tyr-phosphorylated derivatives (Figure 1A). Evaluation of the stability of fibrils formed by these synthetic peptides indicated that the peptide phosphorylated at the N-terminal serine residue showed remarkably low fibrillation propensity as compared to that of the peptide phosphorylated at tyrosine, though these monophosphorylated peptides possessed the same net charge. Analyses of the fibrils by the X-ray fiber diffraction method and Fourier transform infrared (FT-IR) spectroscopic measurements indicated that all the peptides shared a common cross-β structure. Possible protofilament models with four β-sheets were constructed to consider the positional effects of the serine and/or tyrosine phosphorylations. Our results demonstrate that the position of the charged residue, in addition to the previously postulated net charge of the peptide, plays a critical role in amyloid fibrillation of the tau-derived short peptides.

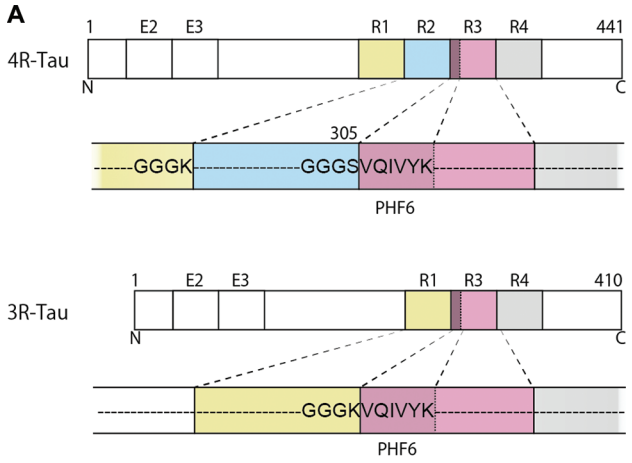

B

$Ac\text{-}X_1VQIVX_2K\text{-}NH_2$

Peptide	X_1	X_2
PHF6	-	Y
PHF6pY	-	pY
SPHF6	S	Y
SPHF6pY	S	pY
pSPHF6	pS	Y
pSPHF6pY	pS	pY
KPHF6	K	Y
KPHF6pY	K	pY

Figure 1. Schematic representation of 4R-tau and 3R-tau isoforms and the amino acid sequences of PHF6 derivative peptides used in this study. (A) Bar diagrams of human tau isoforms. Alterative splicing of tau generates the six isoforms each lacking E2, E3, and R2. Ser305 in 4R-tau is changed to lysine in 3R-tau, lacking R2 via alterative splicing of exon 10. (B) PHF6 derivative peptides used in this study. Position X_1 corresponds to Ser305 of 4R-tau, and this position is replaced with phosphoserine (pS) or lysine (K). Position X_2 corresponds to Tyr310 of 4R-tau, and this is replaced with phosphotyrosine (pY). All the peptides are capped at the N-terminus with an acetyl group (Ac) and modified with a C-terminal amide group (NH_2).

MATERIALS AND METHODS

Materials. Protected Fmoc (9-fluorenylmethoxycarbonyl) amino acids, HBTU [2-(1*H*-benzotriazol-1-yl)-1,1,3,3-tetramethyluronium hexafluorophosphate], 1-hydroxybenzotriazole (HOBt), DIEA (*N*,*N*-diisopropylethylamine), TFA (trifluoroacetic acid), and distilled DMF (*N*,*N*-dimethylformamide) were obtained from Watanabe Chemical Industry. Fmoc-PAL-PEG resin (0.4 mmol/g) was from Applied Biosystems. High-performance liquid chromatography (HPLC) grade acetonitrile (Nacalai tesque) was used for both analytical and preparative HPLC. Reagent grade water was used throughout the experiments. 1,1,1,3,3,3-Hexafluoro-2-propanol (HFIP) and sodium 2,4,6-trinitrobenzenesulfonate (TNBS) were obtained from Wako Chemicals. All other chemicals were reagent grade and used without further purification. A reverse-phase C18

dx.doi.org/10.1021/bi201451z | *Biochemistry* 2012, 51, 1396−1406

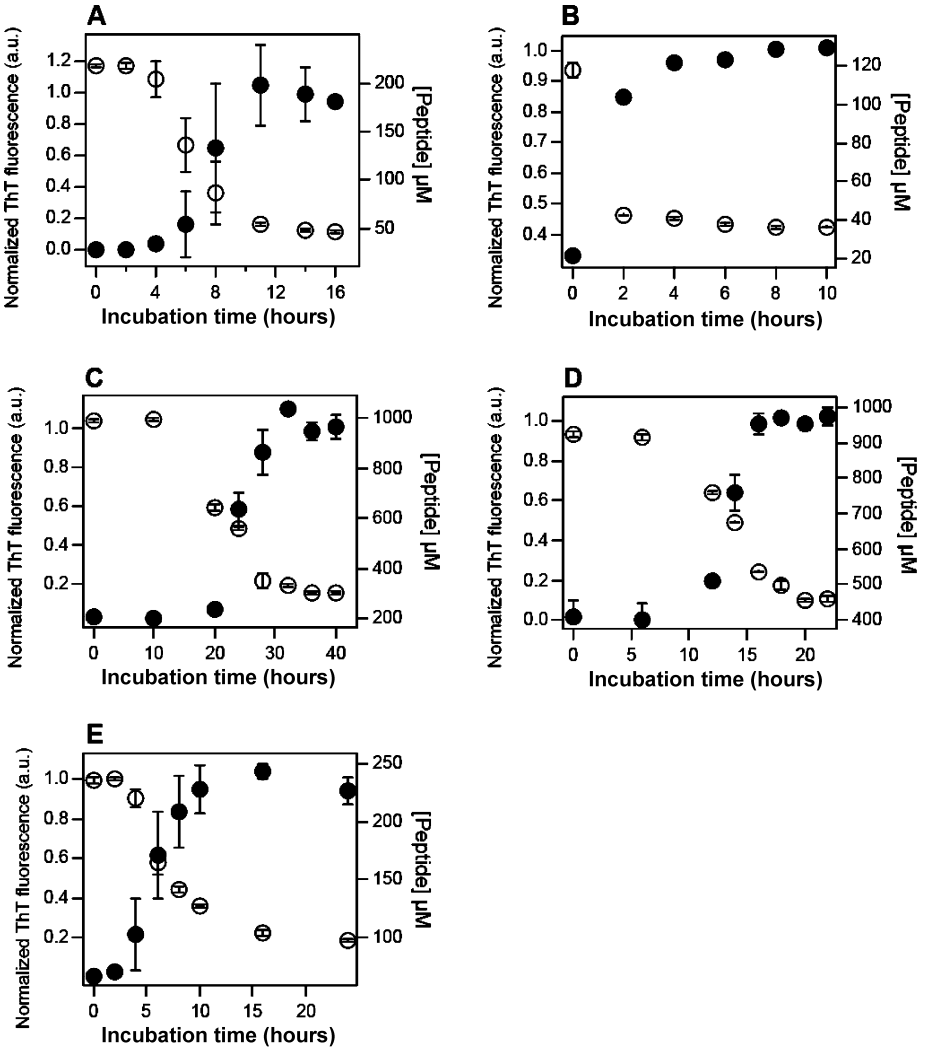

Figure 2. Time course profiles for the changes in ThT fluorescence intensity (●) and the concentration of the residual monomeric peptide in the supernatant (○). The kinetic traces of (A) 200 μM SPHF6, (B) 200 μM SPHF6pY, (C) 1000 μM pSPHF6, (D) 1000 μM KPHF6, and (E) 300 μM KPHF6pY are shown. All the reactions except that depicted in panel D were conducted in the buffer that contained 20 mM MOPS (pH 7.5), 100 mM NaCl, 3% HFIP, and 10 μM ThT. A buffer containing 20 mM glycine (pH 10), 100 mM NaCl, 3% HFIP, and 10 μM ThT was used for the reaction depicted in panel D.

column (20 mm × 250 mm, Ultron VX-Peptide, Shinwa Chemical Industry) and a RESOURCE-RPC column (3 mL, Pharmacia) were used for purification of peptides for preparation. Analytical HPLC was conducted on a reverse-phase C18 column (4.6 mm × 150 mm, Ultron VX-Peptide, Shinwa Chemical Industry). The products were confirmed with an AXIMA MALDI-TOF mass spectrometer (Shimadzu).

Peptide Synthesis and Purification. All peptides were manually synthesized by a solid-phase peptide synthesis method (0.12−0.20 mmol scale). *N*-a-Fmoc-protected amino acids, HBTU (0.6−1.0 mmol, 5 equiv), HOBt (0.6−1.0 mmol, 5 equiv), and diisopropylethylamine (1.2−2.0 mmol, 10 equiv) were used for coupling of protected amino acids. The peptide was cleaved from the resin and deprotected with A (90% TFA/H_2O) or B [TMSBr (trimethylsilyl bromide) (1.35 mL), thioanisole (1.2 mL), 1,2-ethanedithiol (0.6 mL), *m*-cresol (0.2 mL), and trifluoroacetic acid (TFA) (7.48 mL)] depending on the nature of protecting groups. Deprotection of peptides prepared by using Fmoc-Tyr[PO(OBzl)OH]-OH was conducted according to a protocol supplied by Novabiochem. The solution was diluted via addition of diethyl ether to precipitate crude peptides, and the crude sample was collected by centrifugation. The crude peptide was purified with a reverse-phase HPLC system. HPLC conditions: with a C18 column, eluent A, 0.05% TFA/water; eluent B, 0.05% TFA/50% CH_3CN; flow rate of 5 mL/min. The purity of peptides was confirmed by analytical reversed-phase HPLC. The products were characterized by MALDI-TOF MASS. PHF6 (Ac-VQIVYK-NH_2) TOF-MASS: MW calcd 790.96, found 791.09. PHF6pY (Ac-VQIVpYK-NH_2) TOF-MASS: MW calcd 870.94, found 871.07. SPHF6 (Ac-SVQIVYK-NH_2) TOF-MASS: MW calcd 877.04, found 877.12. SPHF6pY (Ac-SVQIVpYK-NH_2) TOF-MASS: MW calcd 957.04.94, found 957.44. pSPHF6 (Ac-pSVQIVYK-NH_2) TOF-MASS: MW calcd 957.04, found 957.56. pSPHF6pY (Ac-pSVQIVpYK-NH_2) TOF-MASS: MW calcd 1037.03, found 1060.03 (Na^+). KPHF6 (Ac-KVQIVYK-NH_2) TOF-MASS: MW calcd 918.13, found 918.12. KPHF6pY (Ac-KVQIVpYK-NH_2) TOF-MASS: MW calcd 997.55, found 997.88. EPHF6 (Ac-EVQIVYK-NH_2) TOF-MASS: MW calcd 919.52, found 919.44. EPHF6pY (Ac-EVQIVpYK-NH_2) TOF-MASS: MW calcd 999.49, found 999.00. Lyophilized peptides were dissolved in HFIP. The

dx.doi.org/10.1021/bi201451z | *Biochemistry* 2012, 51, 1396−1406

Table 1. Critical Concentrations for the Formation of Fibrils of PHF6 Derivative Peptides at Different pH Values

	acidic condition (pH 4.0)		neutral condition (pH 7.5)		basic condition (pH 10.0)	
peptide	net charge	CC (μM)	net charge	CC (μM)	net charge	CC (μM)
PHF6	1	97.2 ± 2.3	1	87.1 ± 3.4	0	66.6 ± 3.9
PHF6pY	0	34.7 ± 2.7	−1	129.1 ± 2.8	−2	257.0 ± 4.6
SPHF6	1	41.3 ± 4.1	1	39.8 ± 1.0	0	18.4 ± 1.8
SPHF6pY	0	23.9 ± 0.2	−1	32.5 ± 0.3	−2	56.2 ± 1.3
pSPHF6	0	237.6 ± 11.6	−1	313.2 ± 7.5	−2	nd[a]
pSPHF6pY	−1	nd[a]	−3	nd[a]	−4	nd[a]
KPHF6	2	nd[a]	2	nd[a]	0	457.7 ± 10.5
KPHF6pY	1	163.2 ± 6.2	0	97.4 ± 1.0	−2	159.7 ± 3.2

[a]Not determined because no significant fluorescence signal could be detected under these conditions.

peptide concentration was determined by using the reported molar extinction coefficients for tyrosine (ε_{275} = 1420 M^{-1} cm^{-1}) and phosphotyrosine (ε_{275} = 500 M^{-1} cm^{-1}) or by quantitation of free amino groups using TNBS. Abbreviations for the amino acids are as follows: E, Glu; S, Ser; I, Ile; K, Lys; Q, Gln; V, Val; Y, Tyr; pY, phosphorylated tyrosine; pS, phosphorylated serine;

Estimation of the Critical Concentration. The peptide stock solution in HFIP was dispensed to a 1.7 mL plastic tube (Sorenson) for adjustment of the final peptide concentration and the final HFIP concentration of 3%. A polymerization reaction was initiated by addition of 20 mM MOPS buffer (pH 7.5), 20 mM acetate buffer (pH 4.0), or 20 mM glycine buffer (pH 10.0) containing 10 μM ThT and 100 mM NaCl. Upon dilution with the buffer, the solution was mixed by gentle pipetting, and 180 μL of the solution was dispensed to the 96-well plate (IWAKI); fibril formation was monitored by thioflavin T (ThT) fluorescence intensities at 480 nm (excitation at 440 nm) with a Wallac ARVOsx 1420 multilabel counter (Perkin Elmer). When the ThT fluorescence intensity reached a plateau, the solution was recovered from the 96-well plate and ultracentrifuged for 1 h at 175000g to remove remaining aggregates in solution. After ultracentrifugation, the supernatant (110 μL) was recovered and the concentration of the peptide was determined by quantitation of free amino groups using TNBS. The TNBS assay took into account the two Lys residues in KPHF6 and KPHF6pY that give twice the signal when normalized for peptide concentration. Under the basic condition, glycine buffer showed a stronger background with the TNBS method, because of the quantitation of peptide concentration achieved by the HPLC method.

Transmission Electron Microscopy (TEM) Measurement. The nanoscale morphology of the peptide aggregates was observed by TEM using a JEM-2000 EX instrument (JEOL, Tokyo, Japan) operated at 200 kV with a magnification of 50000×. The samples prepared in 20 mM MOPS, 100 mM NaCl, 3% HFIP, and 10 μM ThT (pH 7.5), applied to carbon grids, and stained with 2% phosphotungstic acid.

FT-IR Measurements of Peptide Aggregates. FT-IR experiments were performed on an FT/IR-680Plus spectrometer (JASCO, Tokyo, Japan). The sample containing the peptide aggregates was prepared in 20 mM MOPS, 100 mM NaCl, 3% HFIP, and 10 μM ThT (pH 7.5) and then centrifuged at 15000 rpm for 10 min. After the supernatant had been removed, the precipitated aggregates were washed with water twice. The water-rinsed aggregates were spread on a calcium fluoride plate and dried. The measurement was performed at 2 cm^{-1} resolution with accumulation of 128 scans.

X-ray Fiber Diffraction Analyses of Fibrils. The sample preparation was almost the same as that of FT-IR analysis. The water-rinsed aggregates were oriented by repeated pipetting along the wall of the glass capillary and dried. Fibrils on the surface of the glass capillary were exposed to Cu Kα radiation from a MacScience M18XHF rotating-anode generator operating at 45 kV and 90 mA. Images were collected at room temperature with a Bruker Hi-Star multiwire area detector at a sample−detector distance of 130 mm. The d spacing of reflection were calculated using CLEARER.[52]

RESULTS

Evaluation of the Critical Concentration for Fibril Formation by PHF6 Derivative Peptides. PHF6-related peptides containing serine (SPHF6), phosphoserine (pSPHF), and lysine (KPHF6) that represented different charge states at position 305 were synthesized (Figure 1). Other derivatives, SPHF6pY, pSPHF6pY, and KPHF6pY with phosphotyrosine at position X_2, were also synthesized for assessing positional and combinatorial effects of the phosphate group on fibril formation (Figure 1B).

The aggregation propensity of the PHF6 derivatives was first assessed quantitatively by evaluating a critical concentration (C_r)[43] of each peptide for fibril formation. Fibrillation reactions were all initiated by dilution of denatured peptides dissolved in hexafluoro-2-propanol (HFIP) with a buffer containing thioflavin T (ThT) as described previously[20] to ensure reproducible aggregation behavior of each peptide. Time course profiles for the reactions of the fibril growth of PHF6 derivatives were monitored by the change in ThT fluorescence intensity. The fibrillation reaction was first tested with each peptide at 200 μM (Figure S1 of the Supporting Information). When the ThT fluorescence was unchanged after incubation for 24 h, the peptide concentration was sequentially increased to 1000 μM (Figure 2). Buffer solutions of 20 mM MOPS (pH 7.5), 20 mM acetate (pH 4.0), or 20 mM glycine (pH 10.0) were utilized to obtain the critical concentration for each peptide under different pH conditions by considering the pK_a values of the aromatic phosphate group, the aliphatic phosphate group, and the primary amino group are <2 and 5.8, <2 and 6.6, and 10.5, respectively. No phosphate hydrolysis was observed at high or low pH values used in this study.

The kinetic traces for SPHF6, pSPHF6, and KPHF6pY under the neutral condition showed the first delay phase followed by the exponential phase (Figure 2A,C,E), which was typical for nucleation-dependent amyloid-type aggregation.[44−46] No lag phase was observed for the aggregation reaction by SPHF6pY at 200 μM, but the aggregation profile with a lower concentration (150 μM) accompanied a lag phase

dx.doi.org/10.1021/bi201451z | Biochemistry 2012, 51, 1396−1406

in the polymerization reaction (Figure S2 of the Supporting Information). The ThT fluorescence intensity was not changed for KPHF6 (1000 μM) under the neutral condition, but it grew up in the nucleation-dependent manner under the basic condition (Figure 2D). All peptides except for pSPHF6pY exhibited the nucleation-dependent kinetic profile.

The progress of fibril formation was also monitored by the time-dependent change in the concentration of the residual unpolymerized peptide. After ultracentrifugation of an aliquot of the reaction mixture, a peptide concentration in the supernatant of the aliquot was determined by HPLC and by quantification of the free amino groups by sodium 2,4,6-trinitrobenzenesulfonate (TNBS). As shown in Figure 2, the time course profile of the unpolymerized peptide concentration in the supernatant paralleled that of fibril formation obtained by the ThT fluorescence measurement. When the intensity of ThT fluorescence reached a maximum, a plateau value, the peptide concentration in the supernatant also reached a stationary phase, which reflected the status of the dynamic equilibrium between the fibril and the peptide monomer (Table 1). The concentration of the monomer at equilibrium, the critical concentration, corresponds to the fibril dissociation equilibrium constant.[43]

Aggregation Properties of PHF6 Derivatives. The effects of pH conditions were investigated to clarify the relationship between the fibrillation propensities and the charged states of ionic functional groups, such as the phosphate group and the amino group. A net charge of each peptide was calculated as the sum of the positive charge of the amino group of Lys and the negative charge of the phosphorylated residues under each pH condition (Table 1). The positive charge of the side chain of Lys is supposed to be partially reduced at pH 10, which is roughly estimated as zero to count the loss of positive charge at pH 10. Under our experimental conditions, amyloid-like fibrils were formed only for the peptides bearing a net charge that ranged from +1 to −2, and the pH condition at which the net charge of a peptide was closer to zero had a tendency to give a lower C_r value for a given peptide.

When the C_r values of the peptide under different pH conditions were compared, the C_r value for SPHF6 at pH 4.0 was comparable to that at pH 7.5. The net charge of SPHF6 was expected to be +1 at both pH 4.0 and 7.5. SPHF6 revealed the lowest C_r value at pH 10, where the positive charge of the amino group was partially compensated to result in the net charge being near zero. No aggregation of KPHF6 was observed at pH 4.0 and 7.5 where the net charge of KPHF6 was expected to be +2. SPHF6 and KPHF6 containing the amino group of Lys as the sole ionic functional group are prone to forming amyloid fibrils under the basic condition. In contrast, the lowest C_r values for phosphorylated peptides SPHF6pY and pSPHF6 were observed under the acidic condition where the net charge of the peptide approached zero. KPHF6pY showed the lowest C_r value at pH 7.5 where the net charge of the peptide was expected to be zero. KPHF6pY aggregated under the basic condition where the net charge of KPHF6pY was expected to be −2. Thus, the pH-dependent aggregation property of these peptides correlated well with the net charge of the peptides.

Interestingly, SPHF6pY and pSPHF6 showed different aggregation properties despite the fact that they possessed the same net charge. The stability of the aggregates of SPHF6pY was significantly higher than that of pSPHF6 under both the neutral and the acidic conditions. The kinetic profile for the fibril formation of pSPHF6 at a much higher concentration (1000 μM) revealed a longer lag phase of the nucleation (Figure 2C) than 200 μM SPHF6pY. Under the experimental conditions described here, the doubly phosphorylated pSPHF6pY never generated peptide aggregates even under the acidic condition where the net charge of pSPHF6pY was expected to be −1. When the phosphorylated Ser residue of pSPHF6pY was substituted with Lys in KPHF6pY, a dramatic enhancement of the fibrillation propensity was observed especially under the neutral and basic conditions. The fibrillation propensities of EPHF6 (EVQIVYK) and EPHF6pY (EVQIVpYK) peptides possessing the glutamic acid (E) residue as the isostere for the N-terminal phosphoserine were analyzed at pH 4 and 7.5 (Figure S3A of the Supporting Information). Because the pK_a value of Glu is 4.3, the negative charge of the side chain of Glu is expected to be reduced at pH 4.0. EPHF6 exhibited much slower fibril formation that SPHF6 especially at pH 7.5 (Figure S3B of the Supporting Information). Fibril formation of EPHF6 at pH 7.5 was more efficient that that of pSPHF6 at pH 4 (Figure S3B of the Supporting Information), though EPHF6 at pH 7.5 and pSPHF6 at pH 4 would reveal a similar charged state. The negatively charged glutamic acid, like the phosphoserine group, plays an inhibitory role for fibrillation. However, the fibrillation was more strongly inhibited for the peptide possessing the charged phosphoserine group at the N-terminal position (Figure S3B of the Supporting Information). These results indicate that the phosphate group at the N-terminal Ser plays a dominant role in reducing the level of fibrillation of the PHF6 derivatives.

Analyses of the Fibril Morphology by TEM Measurements. The morphologies of the aggregates of PHF6 derivatives at the final plateau phase of the ThT fluorescence assay were analyzed by TEM images (Figure 3). An average

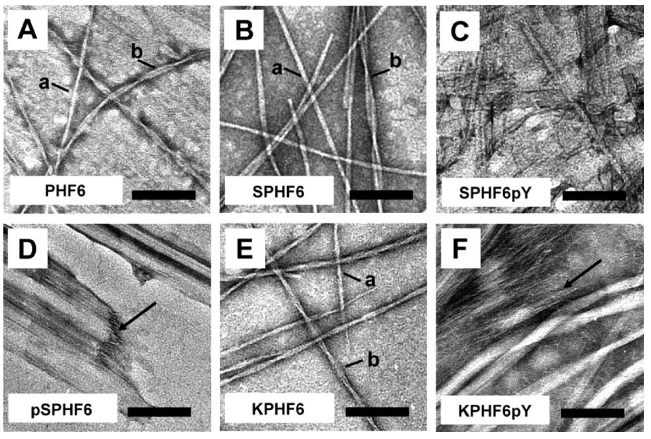

Figure 3. TEM images of fibrous aggregates of PHF6 derivative peptides. Samples at the plateau phase of aggregation kinetics in Figure 2 were used for the measurements: (A) 200 μM PHF6 incubated for 10 h, (B) 200 μM SPHF6 incubated for 10 h, (C) 200 μM SPHF6pY incubated for 10 h, (D) 1000 μM pSPHF6 incubated for 40 h, (E) 1000 μM KPHF6 incubated for 22 h, and (F) 300 μM KPHF6pY incubated for 12 h. Straight filaments or twisted ribbons are marked by a, and paired helical filaments (PHF) are marked by b. Arrows in panels D and F indicate thin filaments with a width of ~4 nm at the termini of fibrils. All samples were transferred directly from the reaction mixture to carbon-coated grids and stained with 2% phosphotungstic acid. The scale bar is 100 nm.

dimension of the fibril of each peptide was determined from ~50 representative fibers in each TEM image and was summarized in Table 2. PHF6 formed the amyloid-type

Table 2. Average Fiber Dimensions from TEM Images for the Fibrils of PHF6 Derivative Peptides

peptide	width[a] (nm)	crossover spacing (nm)	length[d]	morphology
PHF6	6.9 ± 0.6		long	straight or twisted ribbon[e]
	12.5 ± 1.4	63 ± 12[b]	long	paired helical[f]
SPHF6	8.5 ± 0.6		long	straight or twisted ribbon[e]
	16.0 ± 1.0	214 ± 73[b]	long	paired helical[f]
SPHF6pY	11.8 ± 3.2	–	short	segregated mass
pSPHF6	23.3 ± 5.3	–	long	rodlike
KPHF6	7.5 ± 0.5		long	straight or twisted ribbon[e]
	12.0 ± 1.0	71 ± 7[b]	long	paired helical[f]
KPHF6pY	21.3 ± 2.9	nd[c]	long	twisted ribbon

[a]Measured for twisted filaments or helical ribbons. [b]The distances between crossover points of paired-helical filaments. [c]Not determined because no uniform helical period of fibers was observed. [d]Short denotes a fiber length of <1 μm and long a fiber length of <1 μm. [e]Both the straight and twisted ribbonlike filaments were observed. The width of these filaments was almost consistent with the half-width of paired helical filaments. [f]Obvious paired helical filaments in which two filaments wound around each other.

straight or paired helical fibers (Figure 3A) in accordance with previous reports.[20,36,37] SPHF6 also formed straight or paired helical fibers (Figure 3B), while its crossover spacing of 231 nm was larger than that of PHF6 (63 nm). SPHF6pY predominantly provided segregated masses of the fibers with a width of 12 nm and a length of submicrometers (Figure 3C), analogous to those of PHF6pY.[20] The aggregates of pSPHF6 were composed of heterogeneous, rodlike fibers with a mean width of 23.3 nm (Figure 3D). KPHF6 mainly formed paired helical fibers with dimensions similar to those that originated from PHF6 or SPHF6 (Figure 3E). KPHF6pY yielded large helical fibers with a width of 21 nm (Figure 3F). The average widths of the fibers of pSPHF6 and KPHF6pY were considerably larger than those of other peptides. In the TEM images of the fibrils of pSPHF6 and KPHF6pY, thin filaments that have a width of ~4 nm were clearly observed at the termini of fibrils (Figure 3D,F, indicated by arrows), suggesting that interactions between these thin filaments formed the observed thicker fibrils of pSPHF6 and KPHF6pY. The morphologies of aggregates in the initial growth phase for fibrillation were also analyzed by TEM (Figure S4 of the Supporting Information). All peptides formed common-sized short and thin filaments with the diameter of 3–5 nm and/or heterogeneous sphere aggregates. These aggregates mostly disappeared in the sample from the plateau phase of the ThT fluorescence intensity via TEM observation (Figure 3 and Figure S5 of the Supporting Information). The shape of the fibrils changed during the course of the changes in the ThT fluorescence intensity, as revealed for SPHF6 and KPHF6pY (Figure S5 of the Supporting Information). The observed nonfibril types of aggregates would be the intermediates in the formation of mature fibrils.

Structural Characterization of the Fibrils by FT-IR Measurements. The secondary structure of fibrils was analyzed by the FT-IR spectroscopic measurements (Figure 4). The FT-IR spectra showed intense amide I bands around 1630 cm^{-1} characteristic of the β-sheet structure observed for

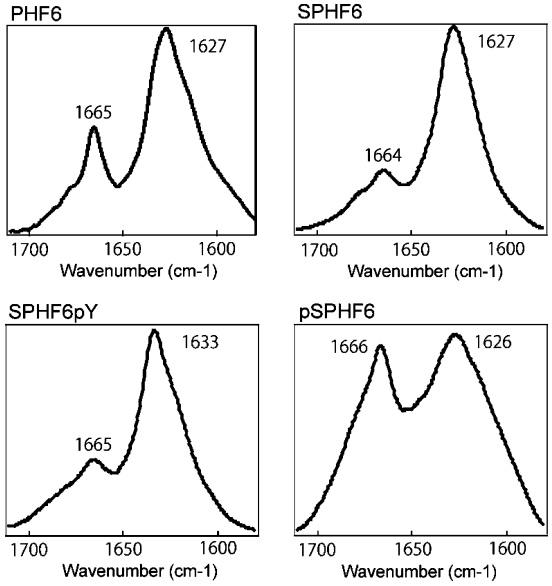

Figure 4. Secondary structure analyses of the PHF6 derivative peptides by FT-IR indicate bands in the amide I region around 1627 cm^{-1} characteristic of the β-sheet secondary structure of PHF6, SPHF6, SPHF6pY, and pSPHF6.

the fibrils of PHF6. No high-frequency component between 1684 and 1704 cm^{-1}, characteristic of an antiparallel strand configuration, was observed, suggesting that these aggregates had a parallel β-sheet configuration.[36,37] While the parallel β-sheet component was predominant in PHF6, SPHF6, and PHF6pY, a broad band around 1666 cm^{-1} was more substantial in the fibril of pSPHF6. Because the band at 1666 cm^{-1} has often been attributed to turn conformations,[47] the aggregates of pSPHF6 may contain oligomeric nonfibrous pSPHF6 that contributes to the spectral absorption.

Structural Characterization of the Fibrils by X-ray Fiber Diffraction Measurements. X-ray fiber diffraction studies were next conducted to characterize the internal structure of the fibrils.[48−52] To prepare partially oriented fiber samples, the wet precipitates collected during the plateau phase of the ThT fluorescence changes (Figure 2) were swabbed on a glass capillary surface in one direction after being washed with water containing 3% HFIP and then dried in air.[53] X-ray diffraction data were successfully obtained from all specimens except for pSPHF6pY. The diffraction patterns (Figure 5, left half of each circle) were compared with a diffraction pattern calculated from the reported microcrystal data of PHF6[35] using CLEARER[52] to elucidate the correlation between the structure of fibrous aggregates and microcrystal structure (Figure 5, right half of each circle, and Figure S6 of the Supporting Information).

Anisotropic X-ray diffraction patterns of the fibrils from PHF6 derivatives closely resembled a typical cross-β pattern that was characterized by a sharp 4.7–4.8 Å meridional and a broader 8–11 Å equatorial reflection.[50,52] The core structure of PHF6 in the microcrystal structure has been identified as a basic unit of two parallel, in-register β-sheets.[35] The calculated diffraction pattern for the two pairs of core β-sheets in the PHF6 microcrystal structure approximately coincided with the

dx.doi.org/10.1021/bi201451z | Biochemistry 2012, 51, 1396–1406

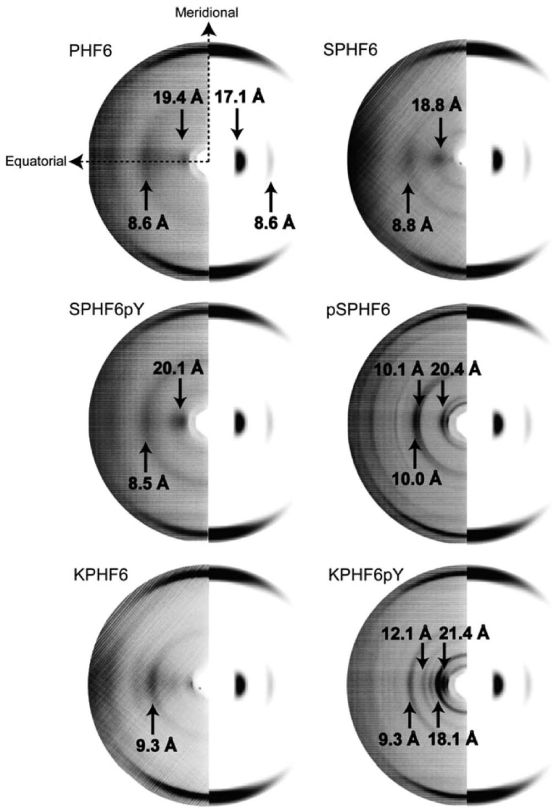

Figure 5. X-ray fiber diffraction patterns of PHF6 derivative peptides. Diffraction patterns were obtained from partially aligned amyloid-type fibrils composed of PHF6, SPHF6, SPHF6pY, pSPHF6, KPHF6, or KPHF6pY. Experimental data (left half) were compared with the calculation pattern (right half) obtained by using CLEARER[52] for the microcrystal structure of PHF6[35] (Figure S2 of the Supporting Information).

observed diffraction pattern for fibrils of SPHF6 (Figure 5). All the diffraction patterns of the PHF6 derivatives showed the sharp and intense reflection at 4.8 Å on the meridian corresponding to the spacing between adjacent hydrogen-bonded β-strands (Table 3). Thus, the β-strands in the fibrils of PHF6 derivatives are oriented perpendicular to the fibril axis with the same atomic spacing that was observed in the microcrystal structure of PHF6 (Figure S6 of the Supporting Information).

Equatorial diffraction peaks for the fibrils of PHF6, SPHF6, SPHF6pY, and KPHF6 that ranged from 8.5 to 9.3 Å would be derived from the lateral packing of the main chains, and these diffraction peaks corresponded to the predicted diffraction of 8.6 Å in the microcrystal structure of PHF6 (Figure 5). These variations in the equatorial reflection imply that the packing arrangement between β-strands in the lateral direction would vary for each peptide. The higher-order broad diffraction peaks for the fibrils of PHF6, SPHF6, SPHF6pY, and KPHF6 around 20 Å may correspond to the distance between the first and third β-sheets. Such a diffraction peak was also observed in the calculated PHF6 diffraction (Figure S6 of the Supporting Information). These results strongly suggest that PHF6, SPHF6, SPHF6pY, and KPHF6 generate fibrous aggregates composed of a common fundamental cross-β unit.

Unlike these peptides, pairs of slightly larger reflections at 10.0 and 10.1 Å for pSPHF6 and at 9.3 and 12.1 Å for KPHF6pY were identified on the equator, suggesting that these fibrils contained two intersheet distances (Figure 5). The high-order reflections at 20.4 Å for pSPHF6 and 21.4 Å for KPHF6pY are coincident with sum of each couple of intersheet distances, 10.0 Å + 10.1 Å for pSPHF6 and 9.3 Å + 12.1 Å for KPHF6pY, respectively. Such diffraction patterns are consistent with the pairing of β-sandwiches, in which an individual β-sheet was paired with both faces of the β-sheet.[54−58]

DISCUSSION

Molecular Basis of Positional and Combinatorial Effects of the Phosphate Group for Amyloid Fibrillation. The fibrils of the PHF6 derivatives exhibited a variety of morphologies and stabilities depending on the phosphorylation status of the peptide despite the fact that all the fibrils formed from the SPHF6 derivatives shared a common cross-β structure. The positional effect of the phosphate group of the phosphorylated SPHF6 derivatives on the fibrillation propensity and fibril morphology is evaluated by possible models representing the fibril core structure of the SPHF6 derivatives in the cross-β and β-sandwich structures with four and eight β-sheets, respectively, shown with the charged amino acid residues (Figure 6). The electrostatic repulsion of the amino group of Lys in SPHF6 would act as a destabilizing factor for the association of monomers as revealed for the case of fibril formation by PHF6.[20] The critical concentration of SPHF6 is decreased under the basic condition that partially reduced the positive charge of the amino group of Lys (Table 1). The fibril formed by SPHF6pY also shows the diffraction pattern and the amide I band characteristic of the cross-β structure consisting of a parallel β-sheet as observed for SPHF6 (Figure 4). The phosphate group of SPHF6pY would enhance the fibril association by making a charge pair with a neighboring Lys (Figure 6) in the same manner previously proposed for PHF6pY.[20] Because the C_r value of SPHF6pY is lower than that

Table 3. Summary of X-ray Spacing (angstroms) for PHF6 Derivative Peptides[a]

	PHF6		SPHF6		SPHF6pY		pSPHF6		KPHF6		KPHF6pY		calculation	
meridional	**4.8**	s	**4.8**	s	**4.8**	s	**4.8**	s	**4.8**	s	**4.8**	s	**4.8**	s
equatorial	19.4	m	18.8	s	20.1	s	20.4	s	14.3	w	21.4	s	17.1	s
	8.6	s	**8.8**	s	**8.5**	s	**10.1**	m	**9.3**	s	18.1	s	**8.5**	s
	5.3	m	5.3	m	5.3	m	**10.0**	s	7.3	w	14.6	w	5.5	w
							7.3	w	5.3	m	12.1	w		
							5.5	m			**9.3**	m		
											7.3	w		
											5.4	w		

[a]The abbreviations for peak intensities were as follows: s, strong; m, moderate; w, weak. Characteristic reflections of the cross-β diffraction pattern are indicated in boldface.

dx.doi.org/10.1021/bi201451z | *Biochemistry* 2012, 51, 1396−1406

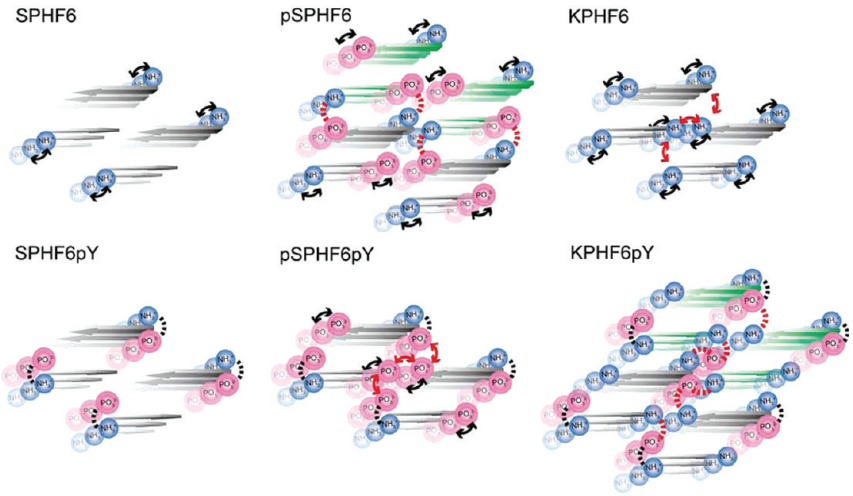

Figure 6. Illustrated models for the fibril core structure of PHF6 derivative peptides representing the possible electrostatic interactions for fibrillation. The charged groups are appended on the β-sheet (gray arrows for a set of four strands and green arrows for another set) with blue spheres representing the positively charged amino group of Lys and the red spheres indicating the negatively charged phosphate group of phosphoserine or phosphotyrosine. Black dashed lines represent the possible electrostatic attraction between the charged groups within the β-strand, and red dashed lines represent the possible intersheet electrostatic attraction between the charged groups. Black arrows denote the possible electrostatic repulsion of charged groups within the β-sheet, and red arrows denote the possible intersheet electrostatic repulsion between the charged groups.

of PHF6pY (Table 1), the hydroxyl group of Ser likely contributes to the stabilization of the fibrils formed by SPHF6pY by an interaction with the negatively charged phosphate group in the lateral direction.

The charge repulsion between the phosphate groups and between the amino groups of Lys at both termini of pSPHF6 in the parallel β-sheet configuration would be unfavorable for the association of monomers by considering a core structure of four sheets. However, excess charges of the phosphate group on phosphoserine and the amino group of Lys are expected to enhance the lateral association between protofilaments to compensate for each other by considering such favorable associations between two sets of the four-sheet core structure (Figure 6). The model based on the pairing of cross β-sandwiches reasonably explains the observed greater width of the pSPHF6 fibril.

In this study, the fibrillation of bis-phosphorylated pSPHF6pY is strongly inhibited even under the acidic pH condition where the net charge of pSPHF6pY is expected to be −1. These two phosphate groups are located close each other in the core structure model of pSPHF6pY considering four β-sheets (Figure 6). Even when the Lys of pSPHF6pY is paired with phosphotyrosine, the electrostatic repulsion between the noncompensated anion of phosphoserine would destabilize the association of pSPHF6pY in the β-sheet configuration. Intersheet contacts might be strongly inhibited because of the electrostatic repulsion or the steric hindrance by two phosphate groups of phosphotyrosine and phosphoserine. In the case of the fibrillation of pSPHF6, the amino group of Lys would be utilized to organize fibrils to compensate for the anionic charges of the phosphate group of phosphoserine. The fibrillation of pSPHF6 is actually inhibited under the basic condition where compensation of the anionic charge of the phosphate group by the amino group of Lys is less effective. These models suggest a role for Lys that interacts with the negatively charged phosphate group of phosphoserine or phosphotyrosine depending on the phosphorylated position of the peptide in the cross-β or β-sandwich configuration. The intersheet electrostatic interaction between the exposed charged groups on the edge of the β-sheet likely controls the association of protofilaments.

The X-ray fiber diffraction pattern of KPHF6pY, the doublet reflection at 9.3 and 12.1 Å, also indicates β-sandwich structure. The β-sandwich structure, in fact, reasonably explains charge paring interactions in the fibril of KPHF6pY (Figure 6, red dashed lines). The charge pairing between the exposed side chains of two Lys residues and phosphotyrosine would allow the lateral association of protofilaments to induce a morphological change. In the case of KPHF6, the absence of such features leads to the formation of simple paired helical filaments.

The results of TEM analysis along with the changes in ThT fluorescence intensity during the course of fibril formation suggested how the fibrils were formed (Figures S4 and S5 of the Supporting Information). SPHF6, SPHF6pY, pSPHF6, KPHF6, and KPHF6pY might form the fibrils via assembly of the thin filaments observed in the initial growing phase as the common core unit of fibrils. We have also analyzed whether the shape of fibrils could change as they mature after reaching the plateau phase of ThT fluorescence intensity changes. KPHF6pY fibrils were notably packed closely with the gradual decrease in the concentration of peptide in the supernatant as compared to that of SPHF6 (Figure S5 of the Supporting Information). This result implied the charged groups such as phosphate groups and amino groups exposed at the outer surface of fibrils may affect the maturing process of fibrils.

The models presented in Figure 6 apply not to the entire tau protein but just to the short PHF6 domain. Further studies are obviously needed to fully understand the actual effect of phosphorylation on the fibril formation mechanism of hyperphosphorylated tau in brain.

Possible Roles of the Ser Phosphorylation in Fibril Formation. The phosphate group at the N-terminal Ser plays a dominant role in reducing the level of fibrillation of the PHF6 derivatives. To develop a rationale for the effect of a negatively charged residue at the N-terminal position of the peptide, we have analyzed fibril formation by EPHF6 and EPHF6pY that

dx.doi.org/10.1021/bi201451z | *Biochemistry* 2012, 51, 1396−1406

possess glutamic acid as the isostere for phosphoserine. As expected, EPHF6 showed much slower fibril formation than SPHF6, especially at pH 7.5 (Figure S3B of the Supporting Information). However, the fibrillation was more strongly inhibited for pSPHF6 possessing the charged phosphoserine group at the N-terminal position. The experiments using the isostere for the N-terminal phosphoserine confirmed that the negative charge of the N-terminal position plays a dominant role in reducing the extent of fibril formation. In addition, not only the negative charge but also the size of the side chain at the N-terminal position would play an important role in fibril formation.

Rousseau et al.[59−61] have proposed that charged amino acid residues existing at the flank of aggregating peptide segments act as the gatekeeper residue that reduces the aggregation property of the peptide segment. The Lys residue effectively acts as the gatekeeper residue because of its positive charge and large conformational entropy. Our results also suggest the role of gatekeeper residues for the PHF6 derivatives. The aggregation property of KPHF6 is significantly lower than that of SPHF6 (Table 1), indicating that the Lys residue at the edge of the β-sheet plays a role as the gatekeeper residue to reduce the aggregation property of the peptide. However, the phosphorylation of Tyr in KPHF6 strongly enhances the fibrillation propensity (Table 1). The results indicate that phosphorylation is an effective way to modulate amyloid fibrillation by canceling the charge repulsion of the side chain of Lys. The N-terminal phosphoserine residue is also considered as a gatekeeper residue. Unlike the case of Lys, the roles of phosphorylation-susceptible amino acid residues as the gatekeeper would be reversibly controlled by phosphorylation−dephosphorylation reactions in the cell.

The importance of charge interaction as the stabilizing factor for amyloid fibrillation has been reported previously,[2,18,19,28,62,63] particularly for the tau protein that possesses many cationic residues in the microtubule-binding domain. Several phosphorylation sites are expected to influence the fibrillation propensity to form the salt bridges.[21] Our results utilizing the model peptides of tau demonstrated that the electrostatic compensation or repulsion of the phosphate group and the amino group of Lys are the critical factors in controling the fibril formation of the tau-derived peptides. Though the Lys residue at the flank of the aggregation sequence has been postulated as the gatekeeper residue for reducing the level of aggregation, the role of such Lys residues would be altered to enhance the aggregation once phosphorylation takes place near the Lys residue. Therefore, the role of hyperphosphorylation for fibril formation of tau should not be considered only from the point of view of altering the net charge of protein. In addition to the many isoforms of tau, post-translational modifications such as phosphorylation would afford many variations of tau that could define a tau code.[64] On the basis of these findings in the model system, positional and combinatorial effects of each phosphorylation should be studied to understand the aggregation property of each form of the hyperphosphorylated tau proteins in the real system.

■ ASSOCIATED CONTENT

Supporting Information

Time course profiles for the change in the ThT fluorescence intensity of PHF6 derivatives (Figure S1), a time course profile for the change in the ThT fluorescence intensity of 150 μM SPHF6pY (Figure S2), fibril formation reactions of EPHF6 and EPHF6pY (Figure S3), TEM images of the peptides in the initial growth phase (Figure S4), time course analyses of the fibrous aggregates by TEM along the kinetic trace of the ThT fluorescence intensity (Figure S5), and the calculated diffraction pattern from one of the molecular configurations of the microcrystal structure of PHF6 (Figure S6). This material is available free of charge via the Internet at http://pubs.acs.org.

■ AUTHOR INFORMATION

Corresponding Author

*Telephone: +81-774-38-3585. E-mail: t-morii@iae.kyoto-u.ac.jp.

Funding

This work was supported in part by the Grants-in-Aid for Scientific Research from the Ministry of Education, Science, Sports and Culture, Japan, to T.M. (20241051) and T.K. (20570149).

Notes

The authors declare no competing financial interest.

■ ACKNOWLEDGMENTS

We thank Professor Bunzo Mikami for access to X-ray fiber diffraction analyses.

■ REFERENCES

(1) Dobson, C. M. (2003) Protein folding and misfolding. *Nature 426*, 884−890.

(2) Chiti, F., and Dobson, C. M. (2006) Protein misfolding, functional amyloid, and human disease. *Annu. Rev. Biochem. 75*, 333−366.

(3) Selkoe, D. J. (1991) The molecular pathology of Alzheimer's disease. *Neuron 6*, 487−498.

(4) Morishima-Kawashima, M., Hasegawa, M., Takio, K., Suzuki, M., Yoshida, H., Titani, K., and Ihara, Y. (1995) Proline-directed and non-proline-directed phosphorylation of PHF-tau. *J. Biol. Chem. 270*, 823−829.

(5) Goedert, M., Spillantini, M. G., Cairns, N. J., and Crowther, R. A. (1992) Tau proteins of Alzheimer paired helical filaments: Aabnormal phosphorylation of all six brain isoforms. *Neuron 8*, 159−168.

(6) Lee, V. M., Balin, B. J., Otvos, L. Jr., and Trojanowski, J. Q. (1991) A68: A major subunit of paired helical filaments and derivatized forms of normal Tau. *Science 251*, 675−678.

(7) Hernandez, F., and Avila, J. (2007) Tauopathies. *Cell. Mol. Life Sci. 64*, 2219−2233.

(8) Gong, C. X., Liu, F., Grundke-Iqbal, I., and Iqbal, K. (2005) Post-translational modifications of tau protein in Alzheimer's disease. *J. Neural Transm. 112*, 813−838.

(9) Bielska, A. A., and Zondlo, N. J. (2006) Hyperphosphorylation of tau induces local polyproline II helix. *Biochemistry 45*, 5527−5537.

(10) Hoffmann, R., Lee, V. M., Leight, S., Varga, I., and Otvos, L. Jr. (1997) Unique Alzheimer's disease paired helical filament specific epitopes involve double phosphorylation at specific sites. *Biochemistry 36*, 8114−8124.

(11) Jicha, G. A., Lane, E., Vincent, I., Otvos, L. Jr., Hoffmann, R., and Davies, P. (1997) A conformation and phosphorylation-dependent antibody recognizing the paired helical filaments of Alzheimer's disease. *J. Neurochem. 69*, 2087−2095.

(12) Arrasate, M., Perez, M., Valpuesta, J. M., and Avila, J. (1997) Role of glycosaminoglycans in determining the helicity of paired helical filaments. *Am. J. Pathol. 151*, 1115−1122.

(13) Kidd, M. (1963) Paired helical filaments in electron microscopy of Alzheimer's disease. *Nature 197*, 192−193.

(14) Perez, M., Valpuesta, J. M., de Garcini, E. M., Quintana, C., Arrasate, M., Lopez Carrascosa, J. L., Rabano, A., Garcia de Yebenes, J., and Avila, J. (1998) Ferritin is associated with the aberrant tau

filaments present in progressive supranuclear palsy. *Am. J. Pathol. 152*, 1531−1539.
(15) Wray, S., Saxton, M., Anderton, B. H., and Hanger, D. P. (2008) Direct analysis of tau from PSP brain identifies new phosphorylation sites and a major fragment of N-terminally cleaved tau containing four microtubule-binding repeats. *J. Neurochem. 105*, 2343−2352.
(16) Santa-Maria, I., Hernandez, F., Martin, C. P., Avila, J., and Moreno, F. J. (2004) Quinones facilitate the self-assembly of the phosphorylated tubulin binding region of tau into fibrillar polymers. *Biochemistry 43*, 2888−2897.
(17) Hanger, D. P., Anderton, B. H., and Noble, W. (2009) Tau phosphorylation: The therapeutic challenge for neurodegenerative disease. *Trends Mol. Med. 15*, 112−119.
(18) Makin, O. S., Atkins, E., Sikorski, P., Johansson, J., and Serpell, L. C. (2005) Molecular basis for amyloid fibril formation and stability. *Proc. Natl. Acad. Sci. U.S.A. 102*, 315−320.
(19) Tjernberg, L., Hosia, W., Bark, N., Thyberg, J., and Johansson, J. (2002) Charge attraction and β propensity are necessary for amyloid fibril formation from tetrapeptides. *J. Biol. Chem. 277*, 43243−43246.
(20) Inoue, M., Hirata, A., Tainaka, K., Morii, T., and Konno, T. (2008) Charge-pairing mechanism of phosphorylation effect upon amyloid fibrillation of human tau core peptide. *Biochemistry 47*, 11847−11857.
(21) Li, W., and Lee, V. M. (2006) Characterization of two VQIXXK motifs for tau fibrillization in vitro. *Biochemistry 45*, 15692−15701.
(22) Hasegawa, M., Morishima-Kawashima, M., Takio, K., Suzuki, M., Titani, K., and Ihara, Y. (1992) Protein sequence and mass spectrometric analyses of tau in the Alzheimer's disease brain. *J. Biol. Chem. 267*, 17047−17054.
(23) Morishima-Kawashima, M., Hasegawa, M., Takio, K., Suzuki, M., Yoshida, H., Watanabe, A., Titani, K., and Ihara, Y. (1995) Hyperphosphorylation of tau in PHF. *Neurobiol. Aging 16*, 365−371.
(24) Hanger, D. P., Betts, J. C., Loviny, T. L., Blackstock, W. P., and Anderton, B. H. (1998) New phosphorylation sites identified in hyperphosphorylated tau (paired helical filament-tau) from Alzheimer's disease brain using nanoelectrospray mass spectrometry. *J. Neurochem. 71*, 2465−2476.
(25) Hanger, D. P., Byers, H. L., Wray, S., Leung, K. Y., Saxton, M. J., Seereeram, A., Reynolds, C. H., Ward, M. A., and Anderton, B. H. (2007) Novel phosphorylation sites in tau from Alzheimer brain support a role for casein kinase 1 in disease pathogenesis. *J. Biol. Chem. 282*, 23645−23654.
(26) Wischik, C. M., Novak, M., Thogersen, H. C., Edwards, P. C., Runswick, M. J., Jakes, R., Walker, J. E., Milstein, C., Roth, M., and Klug, A. (1988) Isolation of a fragment of tau derived from the core of the paired helical filament of Alzheimer disease. *Proc. Natl. Acad. Sci. U.S.A. 85*, 4506−4510.
(27) Wille, H., Drewes, G., Biernat, J., Mandelkow, E. M., and Mandelkow, E. (1992) Alzheimer-like paired helical filaments and antiparallel dimers formed from microtubule-associated protein tau in vitro. *J. Cell Biol. 118*, 573−584.
(28) Fernandez-Escamilla, A. M., Rousseau, F., Schymkowitz, J., and Serrano, L. (2004) Prediction of sequence-dependent and mutational effects on the aggregation of peptides and proteins. *Nat. Biotechnol. 22*, 1302−1306.
(29) Chiti, F., Calamai, M., Taddei, N., Stefani, M., Ramponi, G., and Dobson, C. M. (2002) Studies of the aggregation of mutant proteins in vitro provide insights into the genetics of amyloid diseases. *Proc. Natl. Acad. Sci. U.S.A. 99*, 16419−16426.
(30) Yankner, B. A., Duffy, L. K., and Kirschner, D. A. (1990) Neurotrophic and neurotoxic effects of amyloid β protein: Reversal by tachykinin neuropeptides. *Science 250*, 279−282.
(31) Azriel, R., and Gazit, E. (2001) Analysis of the minimal amyloid-forming fragment of the islet amyloid polypeptide. An experimental support for the key role of the phenylalanine residue in amyloid formation. *J. Biol. Chem. 276*, 34156−34161.
(32) Chiti, F., Stefani, M., Taddei, N., Ramponi, G., and Dobson, C. M. (2003) Rationalization of the effects of mutations on peptide and protein aggregation rates. *Nature 424*, 805−808.
(33) Thompson, M. J., Sievers, S. A., Karanicolas, J., Ivanova, M. I., Baker, D., and Eisenberg, D. (2006) The 3D profile method for identifying fibril-forming segments of proteins. *Proc. Natl. Acad. Sci. U.S.A. 103*, 4074−4078.
(34) Nelson, R., Sawaya, M. R., Balbirnie, M., Madsen, A. O., Riekel, C., Grothe, R., and Eisenberg, D. (2005) Structure of the cross-β spine of amyloid-like fibrils. *Nature 435*, 773−778.
(35) Sawaya, M. R., Sambashivan, S., Nelson, R., Ivanova, M. I., Sievers, S. A., Apostol, M. I., Thompson, M. J., Balbirnie, M., Wiltzius, J. J., McFarlane, H. T., Madsen, A. O., Riekel, C., and Eisenberg, D. (2007) Atomic structures of amyloid cross-β spines reveal varied steric zippers. *Nature 447*, 453−457.
(36) von Bergen, M., Friedhoff, P., Biernat, J., Heberle, J., Mandelkow, E. M., and Mandelkow, E. (2000) Assembly of tau protein into Alzheimer paired helical filaments depends on a local sequence motif (^{306}VQIVYK^{311}) forming β structure. *Proc. Natl. Acad. Sci. U.S.A. 97*, 5129−5134.
(37) Goux, W. J., Kopplin, L., Nguyen, A. D., Leak, K., Rutkofsky, M., Shanmuganandam, V. D., Sharma, D., Inouye, H., and Kirschner, D. A. (2004) The formation of straight and twisted filaments from short tau peptides. *J. Biol. Chem. 279*, 26868−26875.
(38) Rojas Quijano, F. A., Morrow, D., Wise, B. M., Brancia, F. L., and Goux, W. J. (2006) Prediction of nucleating sequences from amyloidogenic propensities of tau-related peptides. *Biochemistry 45*, 4638−4652.
(39) Hirata, A., Sugimoto, K., Konno, T., and Morii, T. (2007) Amyloid-forming propensity of the hydrophobic non-natural amino acid on the fibril-forming core peptide of human tau. *Bioorg. Med. Chem. Lett. 17*, 2971−2974.
(40) Hensley, K., Floyd, R. A., Zheng, N. Y., Nael, R., Robinson, K. A., Nguyen, X., Pye, Q. N., Stewart, C. A., Geddes, J., Markesbery, W. R., Patel, E., Johnson, G. V., and Bing, G. (1999) p38 kinase is activated in the Alzheimer's disease brain. *J. Neurochem. 72*, 2053−2058.
(41) Drewes, G., Ebneth, A., Preuss, U., Mandelkow, E. M., and Mandelkow, E. (1997) MARK, a novel family of protein kinases that phosphorylate microtubule-associated proteins and trigger microtubule disruption. *Cell 89*, 297−308.
(42) Lee, V. M., Goedert, M., and Trojanowski, J. Q. (2001) Neurodegenerative tauopathies. *Annu. Rev. Neurosci. 24*, 1121−1159.
(43) Lomakin, A., Chung, D. S., Benedek, G. B., Kirschner, D. A., and Teplow, D. B. (1996) On the nucleation and growth of amyloid β-protein fibrils: Detection of nuclei and quantitation of rate constants. *Proc. Natl. Acad. Sci. U.S.A. 93*, 1125−1129.
(44) O'Nuallain, B., Shivaprasad, S., Kheterpal, I., and Wetzel, R. (2005) Thermodynamics of Aβ(1−40) amyloid fibril elongation. *Biochemistry 44*, 12709−12718.
(45) Harper, J. D., and Lansbury, P. T. Jr. (1997) Models of amyloid seeding in Alzheimer's disease and scrapie: Mechanistic truths and physiological consequences of the time-dependent solubility of amyloid proteins. *Annu. Rev. Biochem. 66*, 385−407.
(46) Jarrett, J. T., and Lansbury, P. T. Jr. (1993) Seeding "one-dimensional crystallization" of amyloid: A pathogenic mechanism in Alzheimer's disease and scrapie? *Cell 73*, 1055−1058.
(47) Krimm, S., and Bandekar, J. (1986) Vibrational spectroscopy and conformation of peptides, polypeptides, and proteins. *Adv. Protein Chem. 38*, 181−364.
(48) Kirschner, D. A., Inouye, H., Duffy, L. K., Sinclair, A., Lind, M., and Selkoe, D. J. (1987) Synthetic peptide homologous to β protein from Alzheimer disease forms amyloid-like fibrils in vitro. *Proc. Natl. Acad. Sci. U.S.A. 84*, 6953−6957.
(49) Kirschner, D. A., Abraham, C., and Selkoe, D. J. (1986) X-ray diffraction from intraneuronal paired helical filaments and extraneuronal amyloid fibers in Alzheimer disease indicates cross-β conformation. *Proc. Natl. Acad. Sci. U.S.A. 83*, 503−507.
(50) Sunde, M., Serpell, L. C., Bartlam, M., Fraser, P. E., Pepys, M. B., and Blake, C. C. (1997) Common core structure of amyloid fibrils by synchrotron X-ray diffraction. *J. Mol. Biol. 273*, 729−739.

(51) Ivanova, M. I., Sievers, S. A., Sawaya, M. R., Wall, J. S., and Eisenberg, D. (2009) Common core structure of amyloid fibrils by synchrotron X-ray diffraction. *Proc. Natl. Acad. Sci. U.S.A. 106*, 18990−18995.
(52) Jahn, T. R., Makin, O. S., Morris, K. L., Marshall, K. E., Tian, P., Sikorski, P., and Serpell, L. C. (2009) The common architecture of cross-β amyloid. *J. Mol. Biol. 395*, 717−727.
(53) Balbirnie, M., Grothe, R., and Eisenberg, D. S. (2001) An amyloid-forming peptide from the yeast prion Sup35 reveals a dehydrated β-sheet structure for amyloid. *Proc. Natl. Acad. Sci. U.S.A. 98*, 2375−2380.
(54) Serpell, L. C., Fraser, P. E., and Sunde, M. (1999) X-ray fiber diffraction of amyloid fibrils. *Methods Enzymol. 309*, 526−536.
(55) Lim, A., Makhov, A. M., Bond, J., Inouye, H., Connors, L. H., Griffith, J. D., Erickson, B. W., Kirschner, D. A., and Costello, C. E. (2000) Betabellins 15D and 16D, de novo designed β-sandwich proteins that have amyloidogenic properties. *J. Struct. Biol. 130*, 363−370.
(56) Blake, C., and Serpell, L. (1996) Synchrotron X-ray studies suggest that the core of the transthyretin amyloid fibril is a continuous β-sheet helix. *Structure 4*, 989−998.
(57) Malinchik, S. B., Inouye, H., Szumowski, K. E., and Kirschner, D. A. (1998) Structural analysis of Alzheimer's β(1−40) amyloid: Protofilament assembly of tubular fibrils. *Biophys. J. 74*, 537−545.
(58) Lopez De La Paz, M., Goldie, K., Zurdo, J., Lacroix, E., Dobson, C. M., Hoenger, A., and Serrano, L. (2002) De novo designed peptide-based amyloid fibrils. *Proc. Natl. Acad. Sci. U.S.A. 99*, 16052−16057.
(59) Rousseau, F., Serrano, L., and Schymkowitz, J. W. H. (2006) How evolutionary pressure against protein aggregation shaped chaperone specificity. *J. Mol. Biol. 355*, 1037−1047.
(60) Rousseau, F., Schymkowitz, J., and Serrano, L. (2006) Protein aggregation and amyloidosis: Confusion of the kinds? *Curr. Opin. Struct. Biol. 16*, 118−126.
(61) Pedersen, J. S., Christensen, G., and Otzen, D. E. (2004) Modulation of S6 fibrillation by unfolding rates and gatekeeper residues. *J. Mol. Biol. 341*, 575−588.
(62) Konno, T. (2001) Amyloid-induced aggregation and precipitation of soluble proteins: An electrostatic contribution of the Alzheimer's β(25−35) amyloid fibril. *Biochemistry 40*, 2148−2154.
(63) Konno, T., Oiki, S., Hasegawa, K., and Naiki, H. (2004) Anionic contribution for fibrous maturation of protofibrillar assemblies of the human tau repeat domain in a fluoroalcohol solution. *Biochemistry 43*, 13613−13620.
(64) Avila, J. (2009) The tau code. *Front. Aging Neurosci. 1*, 1−5.